

Combined soft and skeletal tissue modeling of normal and dysmorphic midface postnatal development

Amel Ibrahim MB BS ^{a,b}, Michael Suttie MSc ^{a,c}, Neil W Bulstrode MD ^{a,b}, Jonathan A Britto ^b MD, David Dunaway MB ChB BDS ^{a,b}, Peter Hammond PhD ^{a,c*}, Patrizia Ferretti PhD ^{a*}

Institution to which work should be attributed:

UCL Institute of Child Health, University College London
Stem Cells and Regenerative Medicine Section
30 Guilford Street
London WC1N 1EH
United Kingdom
Head of Institute: Professor Rosalind Smyth

Affiliations: ^a UCL Institute of Child Health, University College London, London WC1N 1EH, United Kingdom. ^b Department of Plastic Surgery, Great Ormond Street Hospital NHS Trust, London WC1N 3JH, United Kingdom. ^c Nuffield Department of Obstetrics & Gynaecology, University of Oxford, Oxford OX3 7DQ, United Kingdom.

Corresponding Author*:

Professor Patrizia Ferretti
Stem Cells and Regenerative Medicine Section, UCL Institute of Child Health,
University College London, 30 Guilford Street, London WC1N 1EH,
E-mail: p.ferretti@ucl.ac.uk, Tel: (+44) 020 7905 2372, Fax: (+44) 020 7242 978

Professor Peter Hammond
Nuffield Department of Obstetrics & Gynaecology, University of Oxford, Oxford
OX3 7DQ, United Kingdom
E-mail: peter.hammond@obs-gyn.ox.ac.uk, Tel: +44 (0)1865 617687

Funding Source: This work was funded by the RCS Blond Surgical Research Fellowship (AI) and the National Institute on Alcohol Abuse and Alcoholism (PH and MS: 2U01AA014809). It was also supported by the National Institute for Health Research Biomedical Research Centre at Great Ormond Street Hospital for Children NHS Foundation Trust and University College London.

Combined soft and skeletal tissue modeling of normal and dysmorphic midface postnatal development

Amel Ibrahim MB BS ^{a,b}, Michael Suttie MSc ^{a,c}, Neil W Bulstrode MD ^{a,b}, Jonathan A Britto ^b MD, David Dunaway MB ChB BDS ^{a,b}, Peter Hammond PhD ^{a,c*}, Patrizia Ferretti PhD ^{a*}

Institution to which work should be attributed:

UCL Institute of Child Health, University College London
Stem Cells and Regenerative Medicine Section
30 Guilford Street
London WC1N 1EH
United Kingdom
Head of Institute: Professor Rosalind Smyth

Affiliations: ^a UCL Institute of Child Health, University College London, London WC1N 1EH, United Kingdom. ^b Department of Plastic Surgery, Great Ormond Street Hospital NHS Trust, London WC1N 3JH, United Kingdom. ^c Nuffield Department of Obstetrics & Gynaecology, University of Oxford, Oxford OX3 7DQ, United Kingdom.

Corresponding Author*:

Professor Patrizia Ferretti
Stem Cells and Regenerative Medicine Section, UCL Institute of Child Health, 30 Guilford Street, London WC1N 1EH, United Kingdom
E-mail: p.ferretti@ucl.ac.uk, Tel: (+44) 020 7905 2372, Fax: (+44) 020 7242 978

Professor Peter Hammond
Nuffield Department of Obstetrics & Gynaecology, University of Oxford, Oxford OX3 7DQ, United Kingdom.
E-mail: peter.hammond@obs-gyn.ox.ac.uk, Tel: +44 (0)1865 617687

Funding Source: This work was funded by the RCS Blond Surgical Research Fellowship (AI) and the National Institute on Alcohol Abuse and Alcoholism (PH and MS: 2U01AA014809). It was also supported by the National Institute for Health Research Biomedical Research Centre at Great Ormond Street Hospital for Children NHS Foundation Trust and University College London.

Summary

Midface hypoplasia as exemplified by Treacher Collins Syndrome (TCS) can impair appearance and function. Reconstruction involves multiple invasive surgeries with variable long-term outcomes. This study aims to describe normal and dysmorphic midface postnatal development through combined modeling of skeletal and soft tissues and develop a surgical evaluation tool.

Midface skeletal and soft tissue surfaces were extracted from computed tomography scans of 52 control and 14 TCS children then analysed using dense surface modeling. The model was used to describe midface growth, morphology and asymmetry then evaluate postoperative outcomes.

Parameters responsible for the greatest variation in midface size and shape showed differences between TCS and controls with close alignment between skeletal and soft tissue models. TCS children exhibited midface dysmorphology and hypoplasia when compared with controls. Asymmetry was also significantly higher in TCS midfaces. Combined modeling was used to evaluate the impact of surgery in one TCS individual who showed normalisation immediately after surgery but reversion towards TCS dysmorphology after 1 year.

This is the first quantitative analysis of postnatal midface development using combined modeling of skeletal and soft tissues. We also provide an approach for evaluation of surgical outcomes laying the foundations for future development of a preoperative planning tool.

Keywords

Treacher Collins Syndrome

Development

Dysmorphology

Midface

Dense Surface Modeling

Principal Component Analysis

Introduction

Treacher Collins Syndrome (TCS) is an autosomal dominant disorder of varying penetrance that typifies midface dysmorphia. It has a global incidence of 1:50,000 live births (*Conte et al.*, 2011) and is caused by mutations in the TCOF1 gene. Affected children display various skeletal and soft tissue deformities but downward slanting palpebral fissures and zygomatic hypoplasia, which result in midface deformity, are the most consistent clinical abnormalities (*Teber et al.*, 2004). They have problems with feeding, speech, vision and self-esteem.

Reconstruction usually requires invasive procedures such as distraction-osteogenesis, foreign-body implants and/or tissue transfer (*Cobb et al.*, 2014). These corrections do not completely integrate or grow in harmony with the rest of the face. Thus, surgery is rarely fully or permanently restorative (*Dufresne and Richtsmeier*, 1995).

3-dimensional (3D) reconstructed images from preoperative scans are currently used to plan surgery. Although this increases accuracy, it does not take into account growth and development. Craniofacial bone growth has traditionally been assessed using cephalometric studies (*Bergman et al.*, 2014; *Mellion et al.*, 2013), computed tomography (CT) scans of dry skulls (*Harnet et al.*, 2013; *Nikkhah et al.*, 2013) or indirectly by extrapolating data from soft tissue to the underlying skeleton (*Krimmel et al.*, 2015). Reliance on plain radiographs or CT scans has limited the number of studies that could be undertaken in healthy children who do not normally have such imaging. In contrast, soft tissue growth and morphology has been extensively studied in normal and abnormal development as measurements can be easily obtained through anthropometrics (*Farkas et al.*, 1992; *Tutkuvienė et al.*, 2015) or surface modeling using 3D imaging (*De Souza et al.*, 2013; *Koudelová et al.*, 2015; *Suttie et al.*, 2013). Craniofacial shape and variation can be quantified using morphometric analysis (MA) which has been widely used to study heterogeneity in soft tissues of the face, classify non-genetic diseases, demonstrate normal growth and facial asymmetry and link gene expression

to facial phenotype (*De Souza et al., 2013; Hammond et al., 2003; Hopman et al., 2014*).

Whilst quantitative analysis of the facial skeletal tissues for preoperative planning has been undertaken in TCS, this only used cephalometric analysis or focused on mild dysmorphism (*Chong et al., 2008; Nikkhah et al., 2013*). Hence, computer-aided modeling of severe TCS defects and of the relationship between skeletal and soft tissue shape and growth is still needed to evaluate efficacy of surgery and plan reconstruction.

This study aims to provide a quantitative description of growth and symmetry of normal midface development and assess how this is affected in TCS using the relatively large number of craniofacial CT scans available at Great Ormond Street Hospital (GOSH). We used MA to model the relationship between the shape of skeletal and soft tissues during postnatal midface development. This will form the basis for developing more accurate tools for evaluating and planning midface reconstructive surgery.

Methods

Patient inclusion

Retrospectively collected anonymised CT scans of the face of control and TCS children were acquired from the radiology department at GOSH. Controls were patients coded as not having craniofacial defects and had undergone CT scanning of the head for other reasons (e.g. vascular malformation, oncology or otorhinolaryngology). Children with TCS were identified through international diagnostic clinical codes for the disease and clinic letters cross-checked to ensure that diagnosis was accurate. Confirmation was obtained through the National Research Ethics Service that the study did not require Research Ethics Committee approval as it fulfilled their criteria of “projects using non identifiable data that was routinely collected not for research”.

Image processing and extraction of surfaces

CT scans were converted to DICOM format using OSIRIX[®]. Those unsuitable for analysis (e.g. incomplete imaging of the face) were excluded. 3D STL files of the bone and soft tissue were extracted simultaneously using Invesalius[®] using constant thresholds for volume rendering of bone or soft tissue. These were then edited using Meshlab[®] and VAM[®] to obtain individual surfaces.

Generation of landmarks

Anatomically constant landmarks of the skeletal and soft tissue were identified through review of anatomical textbooks (Gray *et al.*, 2005) and the literature (Hopman *et al.*, 2014; Nikkhah *et al.*, 2013) to ensure chosen landmark reliability and reproducibility. The majority of soft tissue landmarks used were similar to those described previously (Suttie *et al.*, 2013). A new pair of soft tissue landmarks, right and left temporale, were generated by superimposing soft and skeletal tissue surfaces then selecting the soft tissue point directly overlying the temporal fossa. Discrete skeletal landmarks for the zygoma and adjacent maxilla as well as lower portion of the frontal bones were identified using direct and indirect landmarking (Farkas *et al.*, 2004; Farkas *et al.*, 1999; Farkas *et al.*, 2002).

Cephalometric measurements of skeletal and soft tissue CT scan reconstructions

Indirect (cephalometric) measurements of midface width, depth and length were performed by extracting (using software developed in-house) the Euclidean distance between landmarks identified as representative of midface width, length and depth (Budai *et al.*, 2003; Farkas *et al.*, 1992; Farkas *et al.*, 2002; Kolar *et al.*, 1985).

Building of Dense Surface Models

Skeletal and soft tissue landmarks (Table 1; Supplementary figure S1) were used to annotate each of the respective surfaces using software developed in-house Facemark[®] (Suttie *et al.*, 2013) by one individual (AI) and cross-checked by another (MS).

Using the Procrustes algorithm to compute mean landmarks and thin-plate splines, face/skull surfaces were warped to the mean landmarks, which enabled the set of face/skull surfaces to be closely aligned. This allowed points on a selected face/skull to be mapped to closest points on all others to induce a dense surface correspondence of tens of thousands of points enabling computation of the mean midface surface (skeletal or soft). Position differences between the densely corresponded points on each midface surface and those on the mean midface were subjected to Principal Component Analysis (PCA). Principal Components (PCs) accounting for 99% of face variation were used to build a 3D Dense Surface Model (DSM) for synthesis of midface structures (*Hopman et al., 2014*) for skeletal and soft tissues.

Reflection-Original Analysis

Facial asymmetry analysis involved generating a reflected form of each surface and relabeling left-right landmarks before building a DSM of original and reflected midface surfaces (*Hammond et al., 2008*). The Euclidean distance between the DSM representations of the original and reflected faces was used to estimate asymmetry.

Statistical Analysis

Graphpad Prism software was used to generate all charts and graphs apart from 3D scatter plots which were created using SPSS. Linear regression analysis was used to compare the differences between TCS and control children with respect to the first two PCs in the skeletal and soft tissue DSM as well as the asymmetry index. P values were calculated to test whether differences between slopes and intercepts of the regression lines of the TCS and Control subgroups were significant different ($p < 0.05$). Bootstrapping was used to generate confidence intervals for the asymmetry index values in SPSS. Unpaired 2-tailed t-test with Welch's correction was used to analyse mean difference of asymmetry indices and cephalometric measures between the TCS and control subgroups ($p < 0.05$).

Results

Sample characteristics and landmarks used for DSM building

Sixty-eight CT scans of patients (52 controls, 14 preoperative TCS and 2 postoperative TCS) were used to extract a soft tissue and skeletal tissue surface for each patient in this study (Figure 1; Table 1; Supplementary figure S1). Gender ratio was 28:23 (male:female) in control group and 8:6 in the TCS preoperative group. Age was distributed from 1-16 years (Figure, Supplementary figure S2). One TCS male individual had a preoperative (aged 13), immediately postoperative (aged 14) and one year postoperative CT scan (aged 15).

Forty-five skeletal and 24 soft tissue landmarks were used to annotate each skeletal and soft tissue surface respectively building separate skeletal, soft tissue and combined DSMs (Figure 1; Table 1; Supplementary figure S2).

Combined modeling reveals close alignment between skeletal and soft tissue morphology

The first PC (PC1) was responsible for 54%, 58% and 54% of variation in the skeletal, soft tissue and combined models respectively. When plotted against age, PC1 corresponds to overall midface growth (length and width) (Figure 2A; Video 1). In the skeletal model, the PC1-age regression line has a significantly non-zero slope in controls (slope= 0.1795 ± 0.0104 , $p < 0.0001$) and TCS (slope= 0.1727 ± 0.03917 , $p = 0.0009$) indicating a linear relationship between age and PC1. The difference in slopes is not significant ($p = 0.8152$) suggesting similar rates of growth for both groups whilst difference in the intercepts ($p < 0.0001$) reflects reduced midface size in TCS. In the soft tissue model, there is also a linear relationship between age and PC1 (slope= 0.1928 ± 0.0102 ; $p < 0.0001$) in controls and TCS (slope= 0.1383 ± 0.05277 ; $p = 0.0224$) again with similar slopes ($p = 0.1056$) but differing intercepts ($p = 0.0003$). In the combined model, PC1 also relates to age in controls (slope= 0.1896

± 0.009142 , $p < 0.0001$) and TCS (slope= 0.1639 ± 0.04472 , $p = 0.0032$) with lack of difference in slopes ($p = 0.3756$) and significant difference in intercepts ($p < 0.0001$).

PC2 mainly relates to midface width and depth (Figure 2B; Video 2) and accounts for 11%, 12% and 11% of variation in the skeletal, soft tissue and combined models respectively. In the skeletal model, the linear regression line for controls has a significantly non-zero slope (slope= -0.05733 ± 0.01102 , $p < 0.0001$) indicating a direct relationship between age and PC2 which is not the case for TCS (slope= -0.03037 ± 0.07958 , $p = 0.7094$). Controls and TCS do not show significant difference in regression line slope ($p = 0.5516$) but do so for intercept ($p < 0.0001$) likely due to the narrower and shallower midface in TCS. The soft tissue DSM reveals a significant relationship between age and PC2 for controls (slope= -0.07150 ± 0.01841 , $p = 0.0003$) but not for TCS (slope= -0.04613 ± 0.06012 , $p = 0.4577$) with similar slopes ($p = 0.5986$) but different intercepts ($p < 0.0001$). The combined DSM is consistent with the skeletal and soft tissue models demonstrating a linear relationship between age and PC2 in controls (slope= -0.06683 ± 0.01370 , $p < 0.0001$) but not TCS (slope= -0.05497 ± 0.07358 , $p = 0.4694$) without significant difference between TCS and control slopes ($p = 0.7961$) and significant difference in intercepts ($p < 0.0001$).

Bivariate analysis of the first two PCs supports the relationship between skeletal and soft tissue growth and morphology ($p < 0.0001$) shown by the DSM (Supplementary figure S3).

PC3 mainly describes midface width and length (Video 3). Along with PC1 and PC2, the first three PCs account for 70%, 79% and 71% of all shape variation in the skeletal, soft tissue and combined models (Video 1-3). A 3-d scatter plot (Figure 2C) of PC1-3 shows separate clustering of controls and TCS but overlap of 5 TCS individuals who are located within or close to the control data set likely reflecting phenotypic heterogeneity. The similar appearance of the scatter plots of all three DSM suggests that skeletal and soft tissue midface morphology is closely aligned with respect to PC1-3.

Heat maps reveal shape differences in the TCS midface

Heat maps were used to compare a 4 year old with TCS to age-sex-ethnicity-matched controls (n=20) and visually represent the differences described by the DSM (Figure 3A). In the surface normal comparison, the zygomatic and temporal bone regions in the skeletal model and corresponding soft tissue areas (malar and bitemporal) demonstrate malar hypoplasia and bitemporal narrowing (red in Figure 3A) whilst frontal and nasal regions in both models illustrate prominence of the nose (blue in Figure 3A) and relatively (compared with malar region) enlarged forehead which are characteristic of TCS (*Kolar et al., 1985*). In the lateral (X-axis) and vertical (Y-axis) comparisons there is midface narrowing and shortening respectively (red in Figure 3A). Along the depth (Z-axis), the fronto-nasal region shows reduction in depth (red in Figure 3A). As a whole, this individual exhibits midfacial, orbital and zygomatic hypoplasia that is typical of TCS dysmorphism (*Kolar et al., 1985; Kolar et al., 1987*). These typical features were similarly demonstrated using dynamic morph of an older 12 year-old TCS individual (Video 4).

The average TCS midface was generated using the means of the PC values for all of the TCS models and compared with age-sex-ethnicity-matched controls (n=14) to generate a heat map (Figure 3B). The corresponding soft tissue areas reflect malar hypoplasia in the surface comparison (red-yellow in Figure 3B). Enlargement of the fronto-nasal area in the skeletal model corresponds with the relative enlargement of the forehead and prominent nose (blue in Figure 3B) in the soft tissue heat map. Along the X-axis, there is zygomatic narrowing in the skeletal model whilst both skeletal and soft tissue models reveal shortening (red in Figure 3B) along the Y-axis.

Cephalometric analysis of midface soft and skeletal tissue surfaces supports DSM findings

To validate our models, we analysed cephalometric measurements of midface size (width, length and depth) (Table 2, Figure 1). Analysis demonstrates reduction in width of unoperated

TCS midfaces compared with controls in both skeletal ($p=0.0033$) and soft tissue models ($p=0.0009$). Midface depth is also significantly different in skeletal (< 0.0001) and soft tissue (< 0.0001) measurements.

Comparison of preoperative, immediate postoperative and one year postoperative TCS

Heat maps of a male individual with Treacher Collins syndrome reveal zygomatic hypoplasia preoperatively with corresponding loss of soft tissue volume in the malar region (red in Figure 3C(a)) compared with age-sex-ethnicity-matched controls ($n=20$). This patient underwent reconstruction with bone grafts and immediate results show improvement in the skeletal and soft tissue hypoplasia (blue-green in Figure 3C(b)). A year later, the zygomatic bones are corrected but beginning to resorb (green-yellow-red in Figure 3C(c)) and soft tissue appears hypoplastic (red in Figure 3C(c)) compared with immediately postoperative.

This reversion of midface morphology is also reflected in the 3D scatterplots of PC1-3 (Figure 2C). The preoperative TCS individual is initially located amongst the TCS cluster of patients in all 3 scatterplots. Immediately postoperatively, this individual moves closer to the normal dataset within the plot but one year postoperatively, he regresses towards the TCS cluster.

Asymmetry of the midface is increased in TCS

The difference of the PCA representations of original and reflected forms was used to visualize and measure asymmetry of the midface in each individual (Figure 2D). The mean asymmetry index of the midface in the TCS subgroup is significantly higher than in controls in the skeletal ($p<0.0001$) and soft tissue ($p<0.0001$) models. The mean asymmetry index of controls (skeletal=123, Soft tissue=87.59) was compared with that of TCS (skeletal=197.8, soft tissue=123) and demonstrated differences in both skeletal ($p=0.0018$) and soft tissues ($p=0.0033$) (Table 3). Bootstrap confidence intervals for these comparisons did not show any

possible correlation.

Discussion

This study is the first to describe facial growth and morphology in a healthy and syndromic paediatric population using combined skeletal and soft tissue modeling. This builds on the work of Liebrechts et al who showed that surfaces acquired from pre and postoperative CT images can be used to plan mandibular advancement surgery (*Liebrechts et al., 2015*). Their study accurately predicted soft tissue changes post surgery and was validated in another paper published by this group using the same technique to plan bimaxillary correction (*Liebrechts et al., 2015; Liebrechts et al., 2015*). These papers provide important evidence supporting virtual planning of surgery but are limited to non-syndromic adults and adolescents. More recently, Young et al also used CT images to extract soft tissue and skeletal 3D surfaces of the face in patients aged 7-58 (n=175) (*Young et al., 2016*). Using geometric morphometrics, they analysed skeletal and soft tissue shape to show significant covariation providing evidence that skeletal shape can be predicted using soft tissue morphology. Whilst we also built our models using CT reconstructions of skeletal and soft tissue surfaces, we show close alignment between morphology of the midface skeleton and its soft tissue envelope using individual and combined DSM for normal and TCS midface postnatal development. Through this we have quantified changes in midface width, depth and size to describe the skeletal and soft tissue defects in TCS. We also revealed evidence of significant midfacial asymmetry in TCS not previously reported (*Dixon, 1996*). Our results are supported by the findings of anthropometric studies of the face by Kolar et al (*Kolar et al., 1985*) who demonstrated reduced face width, reduced depth and normal length in TCS. Whilst they concisely described the dysmorphism in TCS using well-established protocols, their study only included 6 children and was restricted to soft tissue morphology. Skeletal dysmorphism in TCS was

previously analysed by Nikkhah et al (*Nikkhah et al.*, 2013) who used cephalometric measurements on preoperative CT scans of TCS and control (dry) skulls which were then compared using PCA to quantify the dysmorphism in TCS and attempt virtual normalization. Their study only analysed skeletal models and excluded severe defects. An attempt at correlating skeletal and soft tissue findings in TCS was made by Herlin et al (*Herlin et al.*, 2013) who used CT reconstructions for skeletal analysis and Magnetic Resonance Imaging (MRI) for the soft tissue study (*Herlin et al.*, 2013) to perform surgical simulation. Whilst this presented the first quantitative analysis of subcutaneous soft tissue volume in TCS, limitations included a small sample size on the MRI study (n=2 TCS) and methodology that disallowed direct correlation between skeletal and soft tissues. Additionally, we used our model to compare a pre and postoperative TCS patient against controls to evaluate efficacy of surgery. This demonstrated immediate correction that was not maintained at one year. More CT scans are required to assess whether this is due to the type of surgery performed or limitations in preoperative planning tools and if there will be ongoing reversion to TCS phenotype. Our study is limited by the relatively small sample size especially with regards to the postoperative evaluation patient (n=1). An increased sample size, different surgical procedures and most importantly repeat CT scan data for each individual over a prolonged period of time are needed to build a tool which can model growth trajectories for each child. This would allow identification of the most variable regions in face growth and shape and correlation between the dependent variables. The combined model needs further analysis to accurately assess how it correlates with the individual DSM to understand how changes to the skeletal DSM affect the soft tissue and the reverse. This would permit development of a surgical planning tool with adequate predictive capabilities so that immediate and long-term morphology and growth can be simulated. The increase in sample size and longitudinal data

collection is more easily achievable in the TCS cohort who often have repeat scans but may be difficult with regards to controls thus a multi-center study will be necessary.

Conclusion

This study shows that a combined model can be generated to relate skeletal and soft tissue changes during normal and TCS midface postnatal development. Heat maps and PCA were used to describe the dysmorphism in TCS and evaluate the impact of a common surgical procedure revealing that whilst correction maybe achieved in the short-term, it may not be maintained long-term. This combined approach could eventually be used to develop a surgical planning tool and extended to other parts of the face using similar protocols.

References

- Bergman, R. T., J. Waschak, A. Borzabadi-Farahani and N. C. Murphy: Longitudinal study of cephalometric soft tissue profile traits between the ages of 6 and 18 years. *Angle Orthod* 84:1 48-55, 2014.
- Budai, M., L. G. Farkas, B. Tompson, M. Katic and C. R. Forrest: Relation between anthropometric and cephalometric measurements and proportions of the face of healthy young white adult men and women. *J Craniofac Surg* 14:2 154-161; discussion 162-153, 2003.
- Chong, D. K., D. J. Murray, J. A. Britto, B. Tompson, C. R. Forrest and J. H. Phillips: A cephalometric analysis of maxillary and mandibular parameters in Treacher Collins syndrome. *Plast Reconstr Surg* 121:3 77e-84e, 2008.
- Cobb, A. R., B. Green, D. Gill, P. Ayliffe, T. W. Lloyd, N. Bulstrode and D. J. Dunaway: The surgical management of Treacher Collins syndrome. *Br J Oral Maxillofac Surg* 52:7 581-589, 2014.
- Conte, C., M. R. D'Apice, F. Rinaldi, S. Gambardella, F. Sangiuolo and G. Novelli: Novel mutations of TCOF1 gene in European patients with Treacher Collins syndrome. *BMC Med Genet* 12:125, 2011.
- de Souza, M. A., C. McAllister, M. Suttie, C. Perrotta, T. Mattina, F. Faravelli, F. Forzano, A. Holland and P. Hammond: Growth hormone, gender and face shape in Prader-Willi syndrome. *Am J Med Genet A* 161:10 2453-2463, 2013.
- Dixon, M. J.: Treacher Collins syndrome. *Hum Mol Genet* 5 Spec No:1391-1396, 1996.
- Dufresne, C. and J. T. Richtsmeier: Interaction of craniofacial dysmorphology, growth, and prediction of surgical outcome. *J Craniofac Surg* 6:4 270-281, 1995.
- Farkas, L. G., O. G. Eiben, S. Sivkov, B. Tompson, M. J. Katic and C. R. Forrest: Anthropometric measurements of the facial framework in adulthood: age-related changes in eight age categories in 600 healthy white North Americans of European ancestry from 16 to 90 years of age. *J Craniofac Surg* 15:2 288-298, 2004.
- Farkas, L. G., J. C. Posnick and T. M. Hreczko: Growth patterns of the face: a morphometric study. *Cleft Palate Craniofac J* 29:4 308-315, 1992.
- Farkas, L. G., B. Tompson, J. H. Phillips, M. J. Katic and M. L. Cornfoot: Comparison of anthropometric and cephalometric measurements of the adult face. *J Craniofac Surg* 10:1 18-25; discussion 26, 1999.
- Farkas, L. G., B. D. Tompson, M. J. Katic and C. R. Forrest: Differences between direct (anthropometric) and indirect (cephalometric) measurements of the skull. *J Craniofac Surg* 13:1 105-108; discussion 109-110, 2002.
- Gray, H., S. Standring, H. Ellis and B. K. B. Berkovitz: Gray's anatomy: the anatomical basis of clinical practice. Elsevier Churchill Livingstone, 2005.
- Hammond, P., C. Forster-Gibson, A. E. Chudley, J. E. Allanson, T. J. Hutton, S. A. Farrell, J. McKenzie, J. J. Holden and M. E. Lewis: Face-brain asymmetry in autism spectrum disorders. *Mol Psychiatry* 13:6 614-623, 2008.
- Hammond, P., T. Hutton, S. Maheswaran and S. Modgil: Computational models of oral and craniofacial development, growth, and repair. *Adv Dent Res* 17:61-64, 2003.
- Harnet, J. C., T. Lombardi, A. Manière-Ezvan, E. Chamorey and J. L. Kahn: Transversal craniofacial growth evaluated on children dry skulls using V2 and V3 canal openings as references. *Surg Radiol Anat* 35:9 757-763, 2013.
- Herlin, C., J. C. Doucet, M. Bigorre and G. Captier: Computer-assisted midface reconstruction in Treacher Collins syndrome part 2: soft tissue reconstruction. *J Craniomaxillofac Surg* 41:7 676-680, 2013.

Herlin, C., J. C. Doucet, M. Bigorre, H. C. Khelifa and G. Captier: Computer-assisted midface reconstruction in Treacher Collins syndrome part 1: skeletal reconstruction. *J Craniomaxillofac Surg* 41:7 670-675, 2013.

Hopman, S. M., J. H. Merks, M. Suttie, R. C. Hennekam and P. Hammond: Face shape differs in phylogenetically related populations. *Eur J Hum Genet* 2014.

Kolar, J. C., L. G. Farkas and I. R. Munro: Surface morphology in Treacher Collins syndrome: an anthropometric study. *Cleft Palate J* 22:4 266-274, 1985.

Kolar, J. C., I. R. Munro and L. G. Farkas: Anthropometric evaluation of dysmorphology in craniofacial anomalies: Treacher Collins syndrome. *Am J Phys Anthropol* 74:4 441-451, 1987.

Koudelová, J., J. Dupej, J. Brůžek, P. Sedlak and J. Velemínská: Modelling of facial growth in Czech children based on longitudinal data: Age progression from 12 to 15 years using 3D surface models. *Forensic Sci Int* 248:33-40, 2015.

Krimmel, M., M. Breidt, M. Bacher, S. Müller-Hagedorn, K. Dietz, H. Bühlhoff, S. Reinert and S. Kluba: Three-Dimensional Normal Facial Growth from Birth to the Age of 7 Years. *Plast Reconstr Surg* 136:4 490e-501e, 2015.

Liebrechts, J., T. Xi, M. Timmermans, M. de Koning, S. Bergé, T. Hoppenreijns and T. Maal: Accuracy of three-dimensional soft tissue simulation in bimaxillary osteotomies. *J Craniomaxillofac Surg* 43:3 329-335, 2015.

Liebrechts, J. H., M. Timmermans, M. J. De Koning, S. J. Bergé and T. J. Maal: Three-dimensional facial simulation in bilateral sagittal split osteotomy: a validation study of 100 patients. *J Oral Maxillofac Surg* 73:5 961-970, 2015.

Mellion, Z. J., R. G. Behrents and L. E. Johnston: The pattern of facial skeletal growth and its relationship to various common indexes of maturation. *Am J Orthod Dentofacial Orthop* 143:6 845-854, 2013.

Nikkhah, D., A. Ponniah, C. Ruff and D. Dunaway: Planning surgical reconstruction in Treacher-Collins syndrome using virtual simulation. *Plast Reconstr Surg* 132:5 790e-805e, 2013.

Suttie, M., T. Foroud, L. Wetherill, J. L. Jacobson, C. D. Molteno, E. M. Meintjes, H. E. Hoyme, N. Khaole, L. K. Robinson, E. P. Riley, S. W. Jacobson and P. Hammond: Facial dysmorphism across the fetal alcohol spectrum. *Pediatrics* 131:3 e779-788, 2013.

Teber, O. A., G. Gillessen-Kaesbach, S. Fischer, S. Böhringer, B. Albrecht, A. Albert, M. Arslan-Kirchner, E. Haan, M. Hagedorn-Greiwe, C. Hammans, W. Henn, G. K. Hinkel, R. König, E. Kunstmann, J. Kunze, L. M. Neumann, E. C. Prott, A. Rauch, H. D. Rott, H. Seidel, S. Spranger, M. Sprengel, B. Zoll, D. R. Lohmann and D. Wiczorek: Genotyping in 46 patients with tentative diagnosis of Treacher Collins syndrome revealed unexpected phenotypic variation. *Eur J Hum Genet* 12:11 879-890, 2004.

Tutkuvienė, J., C. Cattaneo, Z. Obertová, M. Ratnayake, P. Poppa, A. Barkus, K. Khalaj-Hedayati, I. Schroeder and S. Ritz-Timme: Age- and sex-related growth patterns of the craniofacial complex in European children aged 3-6 years. *Ann Hum Biol* 1-10, 2015.

Young, N. M., K. Sherathiya, L. Gutierrez, E. Nguyen, S. Bekmezian, J. C. Huang, B. Hallgrímsson, J. S. Lee and R. S. Marcucio: Facial surface morphology predicts variation in internal skeletal shape. *Am J Orthod Dentofacial Orthop* 149:4 501-508, 2016.

Figure legends:

Figure 1: Skeletal and soft tissue 3D reconstructed CT scans annotation.

A) Skeletal and soft tissue 3D reconstructions annotated with landmarks described in Table 1. **B)**

Landmarking for cephalometric measurements. **1:** width (zy-zy). **2:** length (skeletal: gl-ans; soft tissue: gl-sn). **3:** depth (skeletal: ans-m; soft tissue: sn-p); *ans*: anterior nasal spine, *gl*: glabella, *m*: mastoidale, *na*: nasion, *p*: preaurale, *sn*: subnasale, *zy*: zygion.

Figure 2: Comparison of midface morphometry and asymmetry.

A) Growth as indicated by PC1 is reduced in TCS on skeletal ($p < 0.0001$), soft tissue ($p = 0.0003$) and combined

($P < 0.0001$) DSM. **B)** Width and depth indicated by PC2 is reduced in TCS on skeletal

($p < 0.0001$), soft tissue ($P < 0.0001$) and combined ($p < 0.0001$) DSM. **C)** Comparison of pre

and postoperative TCS midfaces using the first 3 PCs shows separate clustering of TCS and

control groups. The preoperative TCS (preop) patient (located amongst TCS group) moves

closer to the controls postoperatively (Postop 1) but regresses to the TCS cluster 1 year

postoperatively (Postop 2). **D-E)** Comparison of midface asymmetry between TCS and

controls using linear regression analysis of the Asymmetry index (AI). Note increased AI in

TCS in (D) skeletal tissues ($p < 0.0001$) and (E) corresponding increase in soft tissue

asymmetry of TCS midfaces ($p < 0.0001$).

Figure 3: Heat map visualisation of TCS midface dysmorphism compared with controls.

A) Dysmorphology in a 4-year old with TCS produces zygomatic and malar hypoplasia

(red-yellow), bitemporal narrowing (red on surface normal (i); red-blue on lateral (ii)) and

down-slanting palpebral fissures (red on vertical (iii)). **B) The average TCS midface (n=14)**

exhibits narrowing and shortening of the zygoma (X and Y-axes) and reduction in fronto-nasal

depth (Z-axis). Surface normal shows malar and zygomatic hypoplasia (yellow-red), increased inter-orbital distance (blue) and nasal bridge prominence (blue). **C) Evaluating surgery in a TCS child:** **a)** Preoperatively there is zygomatic (skeletal), malar, orbital and bitemporal (soft tissue) hypoplasia. **b)** Dysmorphology reduces after surgery. **c)** One year postoperatively there is soft tissue malar and bitemporal hypoplasia compared with (b) but improved overall compared with preop (a). *Controls (n=20). Heat maps demonstrate difference between TCS and controls on surface normal comparison and along the X, Y and Z axes. Red-green-blue scale indicates a contraction-coincidence-expansion of 2 standard deviations (Stdv) from the mean in the surface-normal comparison.*

Tables

Table 1: Description of landmarks used to annotate midface surfaces.

	Skeletal landmark	Definition	
Unpaired	1. Glabella	Midway between the supraorbital notches	
	2. Nasion	Midpoint of frontonasal suture	
	3. Rhinion	Most anterior-inferior point of nasal suture	
	4. Anterior nasal spine	Apex of anterior nasal spine of maxilla	
	5. Interdentale superius	Between the upper two incisors	
Paired	6. Supraorbital foramen	Most concave point of supraorbital notch	
	7. Supraorbital margin	Midpoint of the orbital rim	
	8. Anterior frontozygomatic	Most anterior point of frontozygomatic suture	
	9. Posterior frontozygomatic	Most posterior point of frontozygomatic suture	
	10. Lateral frontonasal suture	Most lateral point of frontonasal suture	
	11. Orbitale	Most inferior portion of lower orbital rim	
	12. Maxillary process	Most superior part of zygomaticomaxillary suture	
	13. Infraorbital foramen	Most concave point below infraorbital margin	
	14. Ectoconchion	Point of maximum breadth on lateral wall of orbit	
	15. Jugale	Junction of the temporal and frontal processes	
	16. Infratemporal fossa	Midpoint of cavity deep to Zygomatic arch	
	17. Zygomaxillare	Most inferior tip of zygomaticomaxillary suture	
	18. Mastoidale	Lowest point on the contour of the mastoid process	
	19. Canine fossa	Depression lateral to canine eminence	
	20. Tuberosity of maxilla	Lowest part of the infratemporal surface of maxilla	
	21. Zygion	Most lateral point on outline of Zygoma	
	22. Inferior orbital fissure	Apex of sphenomaxillary suture	
	23. Alare	Most lateral point of nasal aperture	
	24. Articular tubercle	Inferior and proximal eminence of zygomatic process	
	25. Postglenoid tubercle	Inferior distal projection of zygomatic process	
		Soft tissue landmark	Definition
	Unpaired	1. Glabella	Most prominent point of frontal bone in the midline
		2. Nasion*	Midline of frontonasal suture
		3. Pronasale	Most prominent point on nasal tip
		4. Subnasale	Midpoint of columella base
Paired	5. Palpebrae superius	Midpoint of superior aspect of palpebral fissure	
	6. Frontotemporale*	Concavity above supraorbital rim	
	7. Endocanthion	Most medial point of palpebral fissure	
	8. Exocanthion	Most lateral point of palpebral fissure	
	9. Palpebrae Inferius	Midpoint of inferior aspect of palpebral fissure	
	10. Zygion*	Most lateral extents of zygoma	
	11. Subaurale	Most inferior point of the free auricular margin	
	12. Preaurale	Most anterior part of the ear	
	13. Alare	Lateral extent of alar contour	
	14. Lateral pronasale	Most distal point of alar groove	

* Landmarks were obtained by superimposing soft tissue surface onto skeletal and projecting the landmark (see Supplementary Figure S1).

Table 2: Differences in cephalometric measurements between control and Treacher Collins (TCS) midface reconstructions.

Measurements (corresponding landmarks)	Skeletal			Soft tissue		
	Controls (n=52)	Unoperated TCS (n=14)	P-values	Controls (n=52)	Unoperated TCS (n=14)	P-values
Midface width (zy-zy)	106.8 ± 1.279	90.55 ± 4.475	0.0033*	125.0 ± 2.828	102.1 ± 5.194	0.0009*
Midface length (Soft tissue: gl-sn; Skeletal: gl-ans)	51.80 ± 0.	48.46 ± 2.116	0.1665	58.08 ± 1.199	54.75 ± 2.682	0.2714
Midface depth† (Soft tissue: sn-p; Skeletal: ans-m)	91.24 ± 1.018	81.09 ± 1.939	< 0.0001*	108.0 ± 1.150	92.13 ± 2.056	< 0.0001*

†For depth both left and right-sided measurements were analysed. The landmarks are as defined in Table 1 (**ans**: anterior nasal spine, **gl**: glabella, **m**: mastoidale, **na**: nasion, **p**: preaurale, **sn**: subnasale, **zy**: zygion). Values shown are means ± SEM; * statistically significant; P-values are from unpaired two-tailed T-test.

Table 3: Comparison of the mean asymmetry indexes of the control and Treacher Collins Syndrome (TCS) groups in the skeletal and soft tissue models and bootstrap confidence intervals.

Group	Skeletal			Soft tissue		
	Controls (n=52)	Unoperated TCS (n=14)	P-value	Controls (n=52)	Unoperated TCS (n=14)	P-value
Mean ± SEM	123.00 ± 4.89	197.80 ± 19.11	0.0018*	87.59 ± 4.14	123.3 ± 9.697	0.0033*
BCa 95% LCI	113.83	164.28	NA	79.09	107.3732	NA
BCa 95% UCI	131.55	232.55	NA	95.85	140.3852	NA

Bca: Bias-corrected and accelerated; LCI: Lower Confidence Interval ± STD; Upper Confidence Interval ± STD; * statistically significant (unpaired two-tailed T-test).

Legends for supplementary figures and videos

Supplementary figure S1: **A)** CT scans of the craniofacial region were volume rendered to extract skeletal and soft tissue surfaces using defined thresholds. Axial, coronal and sagittal sections through the face illustrate the alignment between the skeletal and corresponding soft tissue surfaces. **B)** Use of skeletal landmarks to determine soft tissue landmarks by superimposing the surfaces. **C)** Contour used to position landmarks defined by curvature.

Supplementary figure S2: Age distribution of participants. There are 14 unoperated Treacher Collins Syndrome (TCS) cases, 2 post-operative TCS scans (from the same individual; immediately and 1 year on) and 52 controls. Mean age in years of controls is 8.48 ± 4.55 STD and unoperated TCS is 6.92 ± 4.38 STD.

Supplementary figure S3: bivariate analysis of soft tissue and skeletal tissue growth as described by PC1. **A)** Soft tissue face growth demonstrates a relationship with underlying skeletal growth when PC1 (A) and PC2 (B) values from the skeletal DSM are plotted against those of the soft tissue DSM for each patient ($p < 0.0001$). There is no difference in intercepts or slopes between controls and TCS in **A)** PC1 ((pooled slope= 0.96995 , $p = 0.39$; pooled Y intercept= -0.0477246 , $p = 0.904$) and **B)** PC2 (pooled slope= 0.845484 , $p = 0.0748$; pooled Y intercept= -0.00936876 , $p = 0.1983$).

Video 1: Principal Component 1. Dynamic morphs reveal the change in midfacial appearance that are described by PC1, which relates to overall face size and is associated with age in our DSM (± 2 STD). The relationship between growth and morphology in the skeletal and soft tissues can also be seen.

Video 2: Principal Component 2. Video shows that PC2 is associated with midface width and depth, which is revealed by dynamic morphing of the surfaces in our model (± 2 STD). The relationship between the skeletal and soft tissues changes can also be seen.

Video 3: Principal component 3. Dynamic morphing of the midface surfaces reveals the association between midface width and length with PC3 (± 2 STD). There is also evidence of overlap between the changes described by all 3 PCs. The relationship between the skeletal and soft tissues can also be seen.

Video 4: Changes between a surface model of a 12 year old with TCS and age-sex-gender matched controls. Dynamic morphing demonstrates how the midface morphology changes from controls (n=18) to a surface model of a 12-year old male with TCS. On the skeletal model there is hypoplasia of the zygoma, increased interorbital distance and down slanting of the lateral orbital wall. There is corresponding malar hypoplasia, widening intercanthal distance and increased prominence of the nose on the soft tissue model.

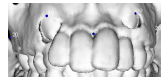
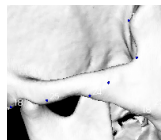
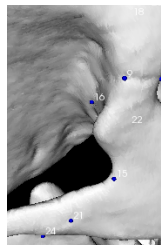
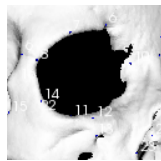
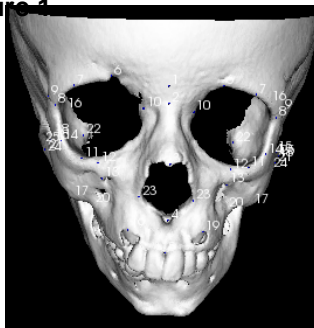
Table 1	Skeletal landmark	Definition
Unpaired	1. Glabella	Midway between the supraorbital notches
	2. Nasion	Midpoint of frontonasal suture
	3. Rhinion	Most anterior-inferior point of nasal suture
	4. Anterior nasal spine	Apex of anterior nasal spine of maxilla
	5. Interdentale superius	Between the upper two incisors
Paired	6. Supraorbital foramen	Most concave point of supraorbital notch
	7. Supraorbital margin	Midpoint of the orbital rim
	8. Anterior frontozygomatic	Most anterior point of frontozygomatic suture
	9. Posterior frontozygomatic	Most posterior point of frontozygomatic suture
	10. Lateral frontonasal suture	Most lateral point of frontonasal suture
	11. Orbitale	Most inferior portion of lower orbital rim
	12. Maxillary process	Most superior part of zygomaticomaxillary suture
	13. Infraorbital foramen	Most concave point below infraorbital margin
	14. Ectoconchion	Point of maximum breadth on lateral wall of orbit
	15. Jugale	Junction of the temporal and frontal processes
	16. Infratemporal fossa	Midpoint of cavity deep to Zygomatic arch
	17. Zygomaxillare	Most inferior tip of zygomaticomaxillary suture
	18. Mastoidale	Lowest point on the contour of the mastoid process
	19. Canine fossa	Depression lateral to canine eminence
	20. Tuberosity of maxilla	Lowest part of the infratemporal surface of maxilla
	21. Zygion	Most lateral point on outline of Zygoma
	22. Inferior orbital fissure	Apex of sphenomaxillary suture
	23. Alare	Most lateral point of nasal aperture
	24. Articular tubercle	Inferior and proximal eminence of zygomatic process
	25. Postglenoid tubercle	Inferior distal projection of zygomatic process
	Soft tissue landmark	Definition
Unpaired	1. Glabella	Most prominent point of frontal bone in the midline
	2. Nasion*	Midline of frontonasal suture
	3. Pronasale	Most prominent point on nasal tip
	4. Subnasale	Midpoint of columella base
Paired	5. Palpebrae superius	Midpoint of superior aspect of palpebral fissure
	6. Frontotemporale*	Concavity above supraorbital rim
	7. Endocanthion	Most medial point of palpebral fissure
	8. Exocanthion	Most lateral point of palpebral fissure
	9. Palpebrae Inferius	Midpoint of inferior aspect of palpebral fissure
	10. Zygion*	Most lateral extents of zygoma
	11. Subaurale	Most inferior point of the free auricular margin
	12. Preaurale	Most anterior part of the ear
	13. Alare	Lateral extent of alar contour
	14. Lateral pronasale	Most distal point of alar groove

Table 2	Skeletal			Soft tissue		
Measurements (corresponding landmarks)	Controls (n=52)	Unoperated TCS (n=14)	P-values	Controls (n=52)	Unoperated TCS (n=14)	P-values
Midface width (zy-zy)	106.8 ± 1.279	90.55 ± 4.475	0.0033*	125.0 ± 2.828	102.1 ± 5.194	0.0009*
Midface length (Soft tissue: gl-sn; Skeletal: gl-ans)	51.80 ± 0.9531	48.46 ± 2.116	0.1665	58.08 ± 1.199	54.75 ± 2.682	0.2714
Midface depth† (Soft tissue: sn-p; Skeletal: ans-m)	91.24 ± 1.018	81.09 ± 1.939	< 0.0001*	108.0 ± 1.150	92.13 ± 2.056	< 0.0001*

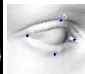
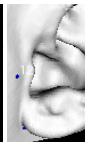
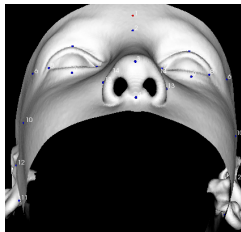
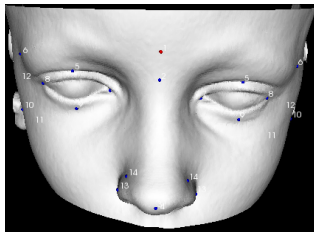
Table 3	Skeletal			Soft tissue		
Group	Controls (n=52)	Unoperated TCS (n=14)	P-value	Controls (n=52)	Unoperated TCS (n=14)	P-value
Mean \pm SEM	123.00 \pm 4.89	197.80 \pm 19.11	0.0018*	87.59 \pm 4.14	123.3 \pm 9.697	0.0033*
BCa 95% LCI	113.83	164.28	NA	79.09	107.3732	NA
BCa 95% UCI	131.55	232.55	NA	95.85	140.3852	NA

Figure 4

Skeletal

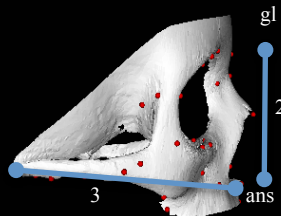
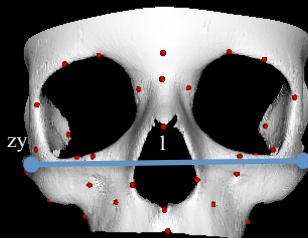


Soft Tissue

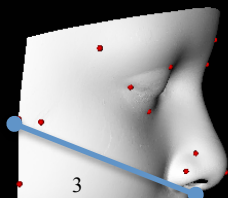
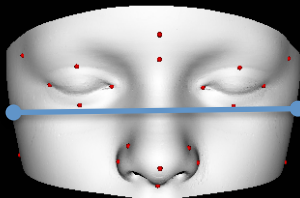


B

Skeletal



Soft Tissue



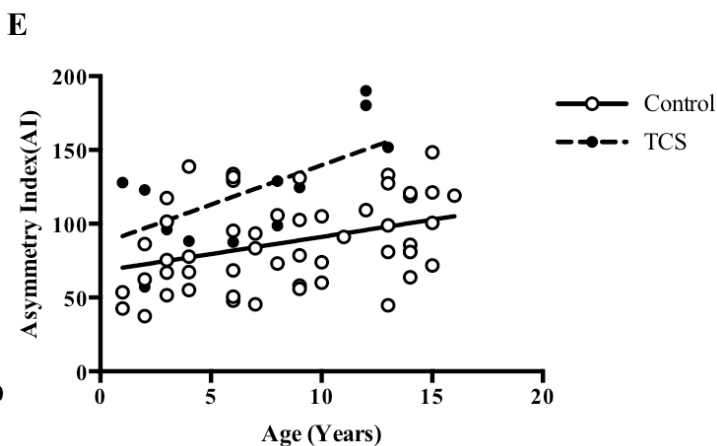
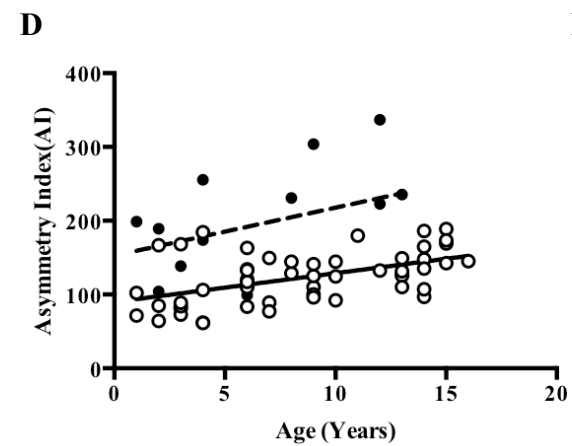
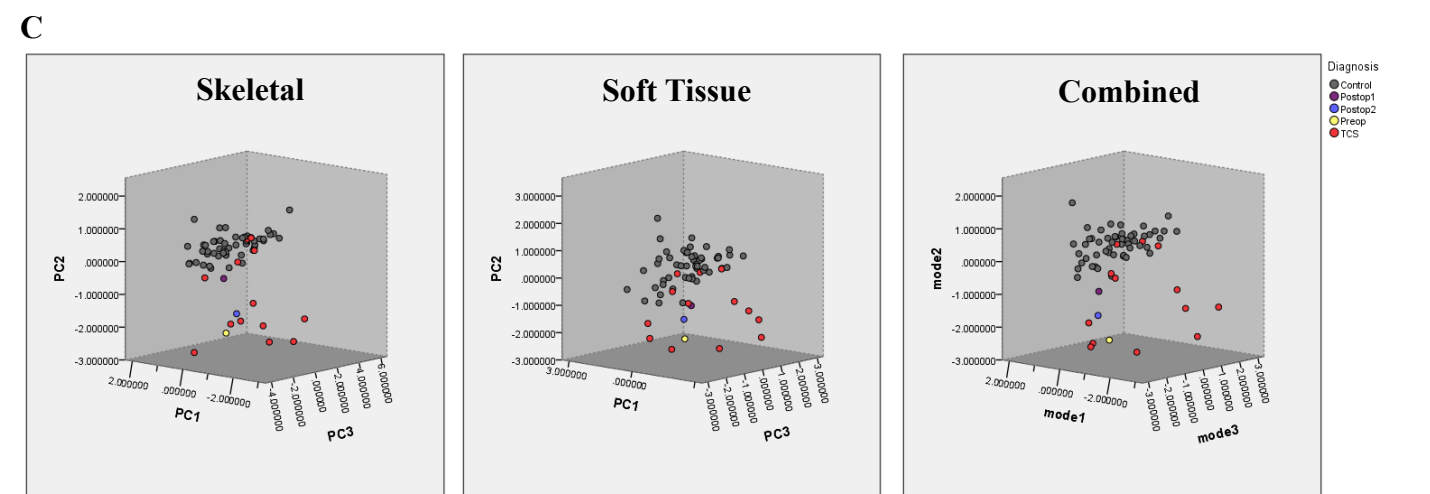
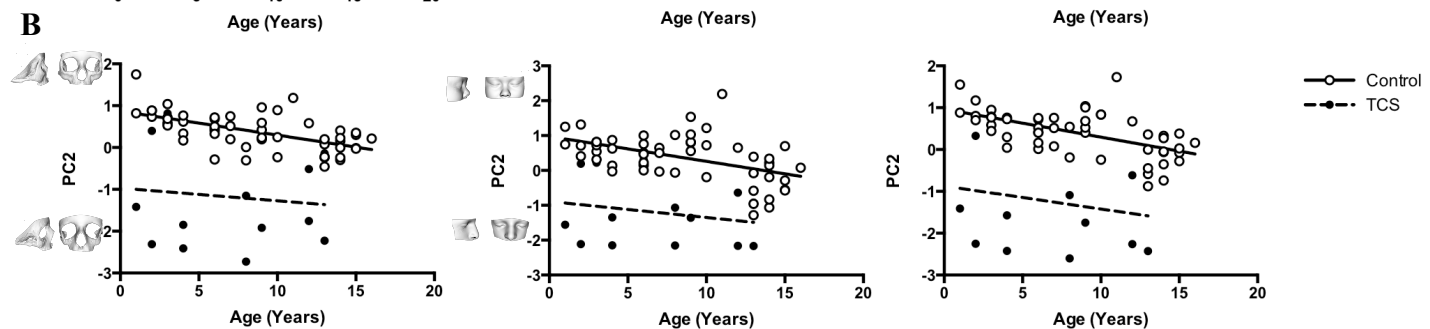
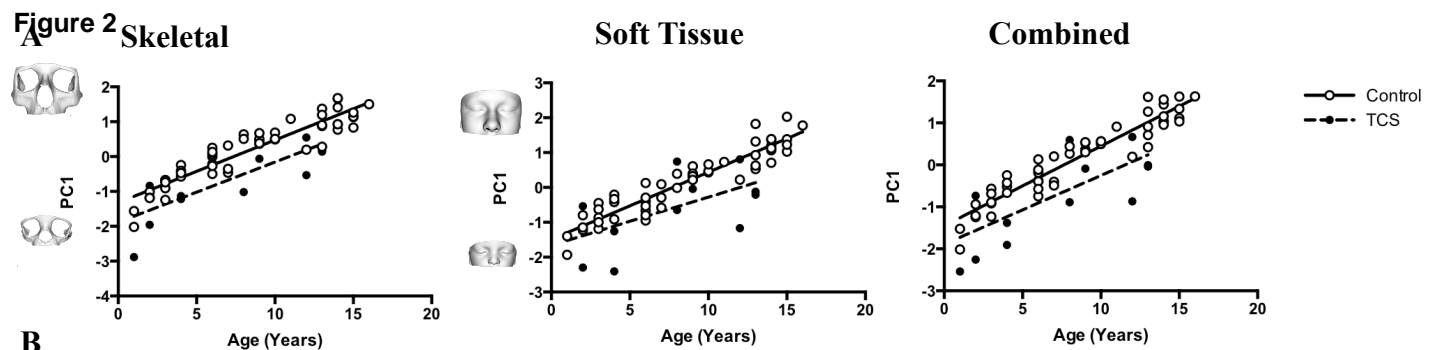
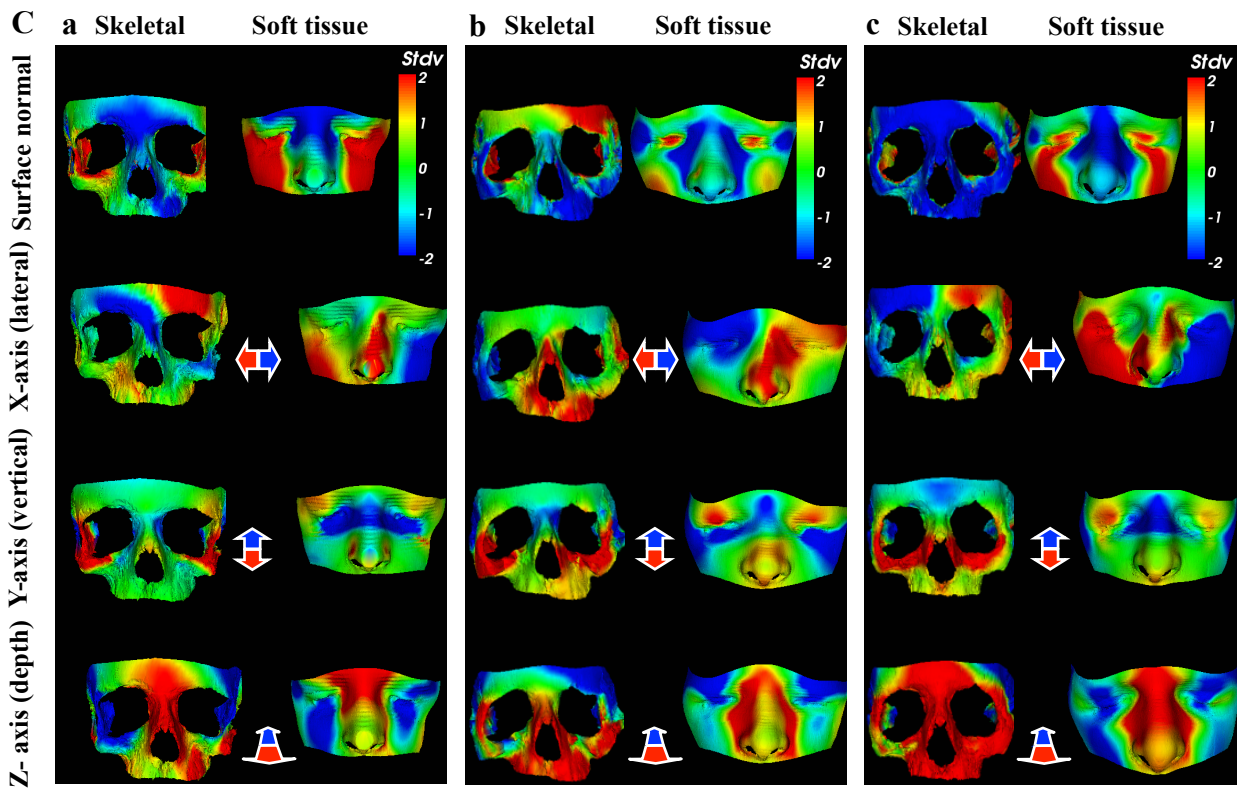
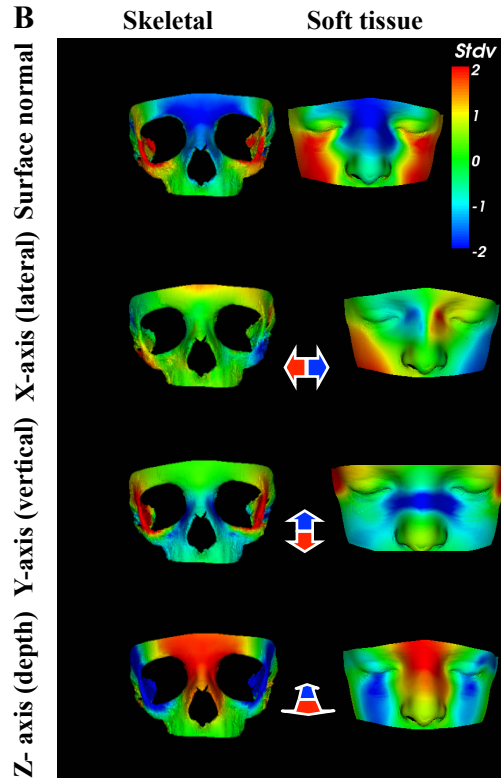
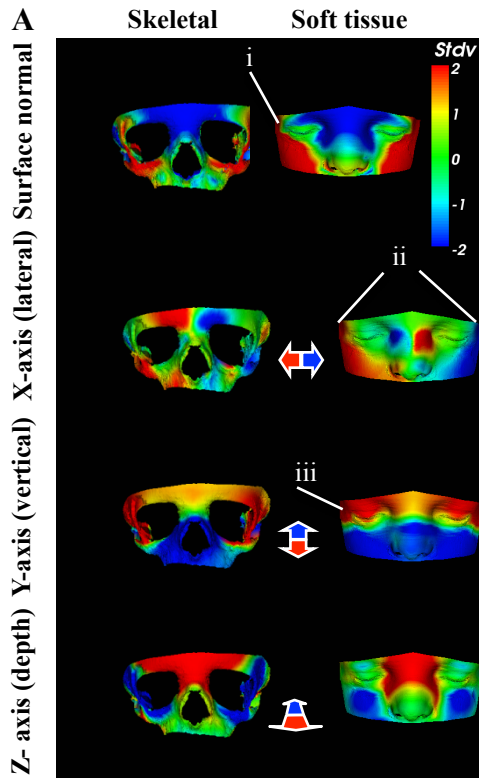
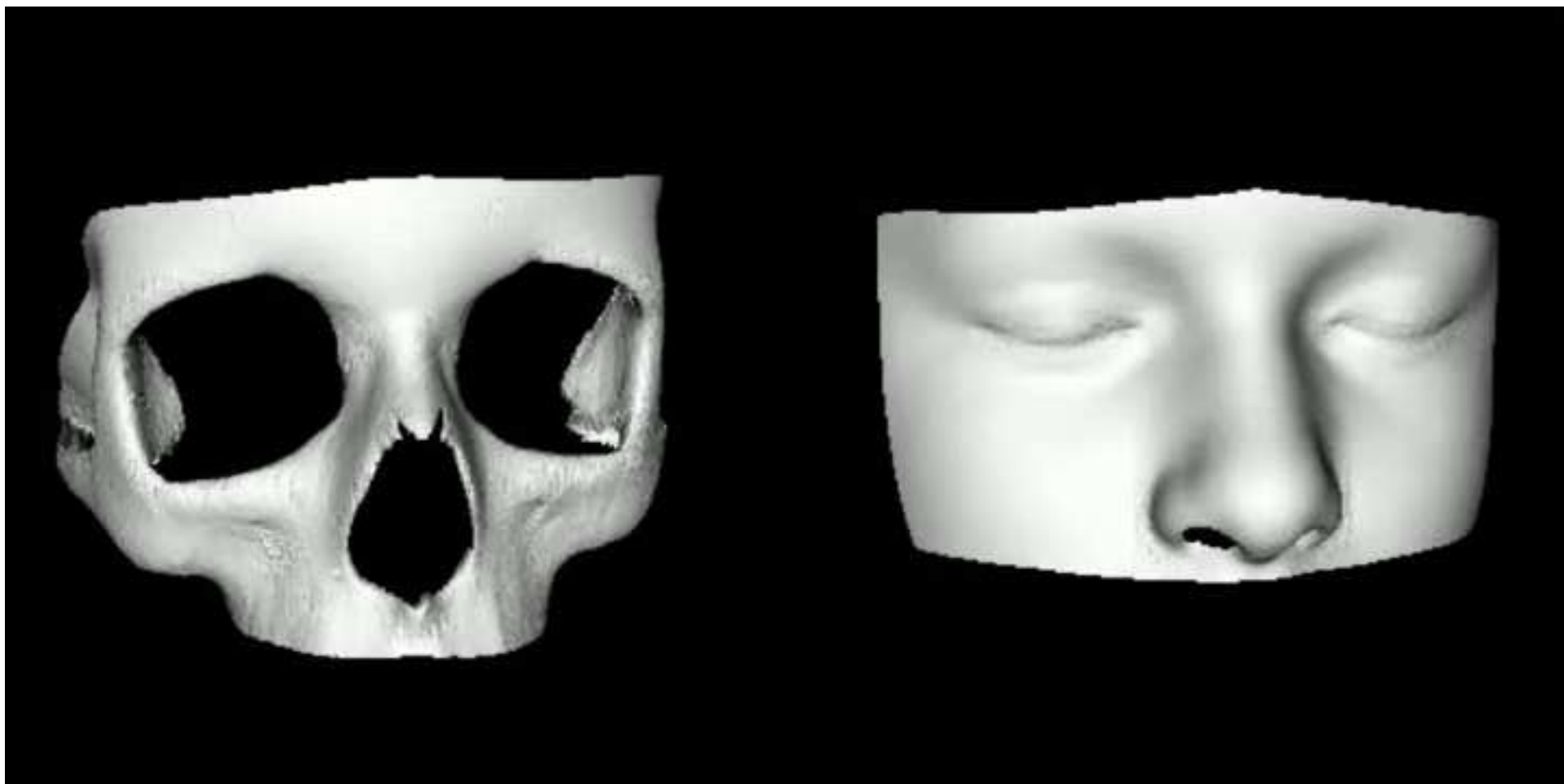
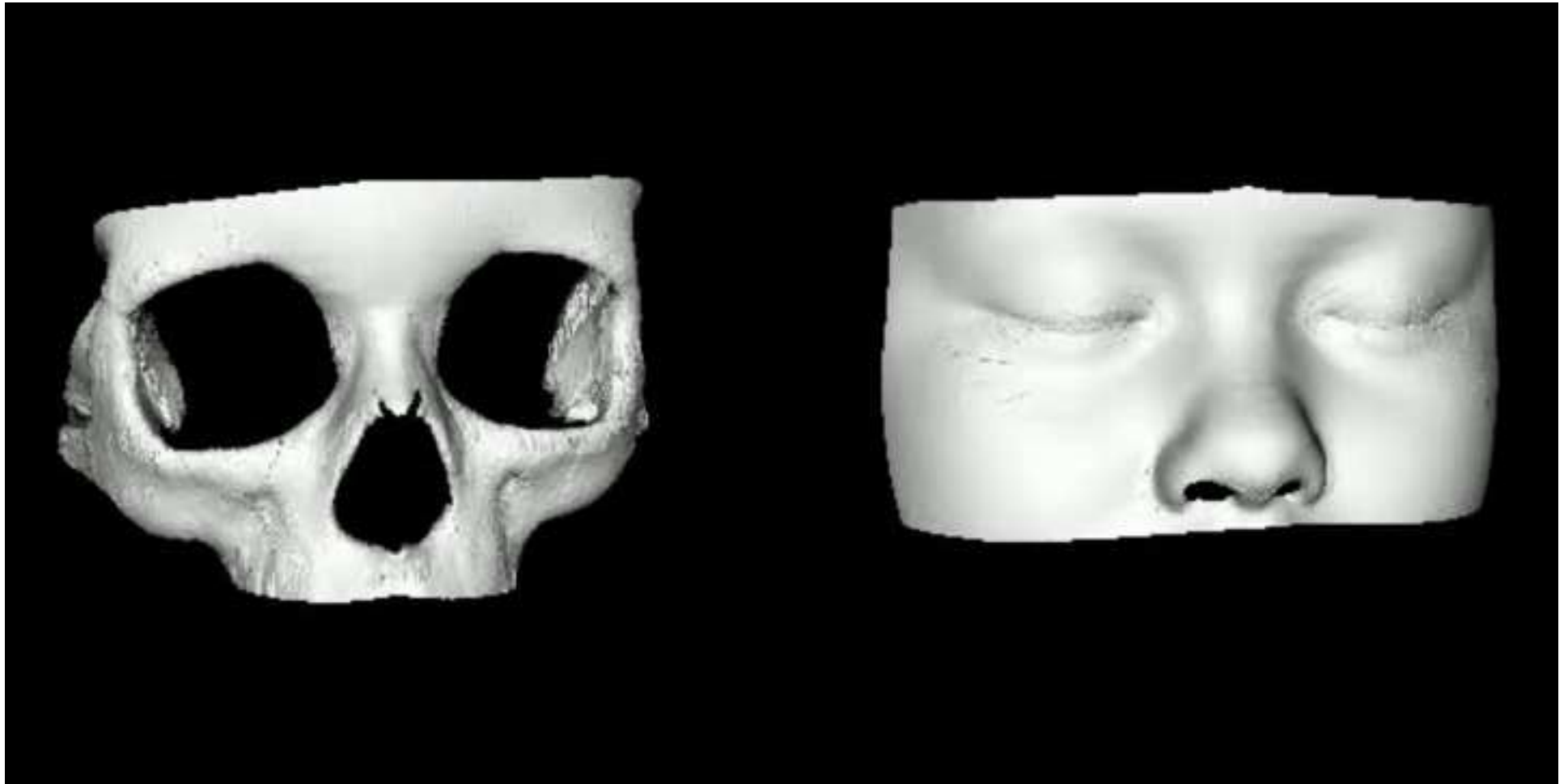
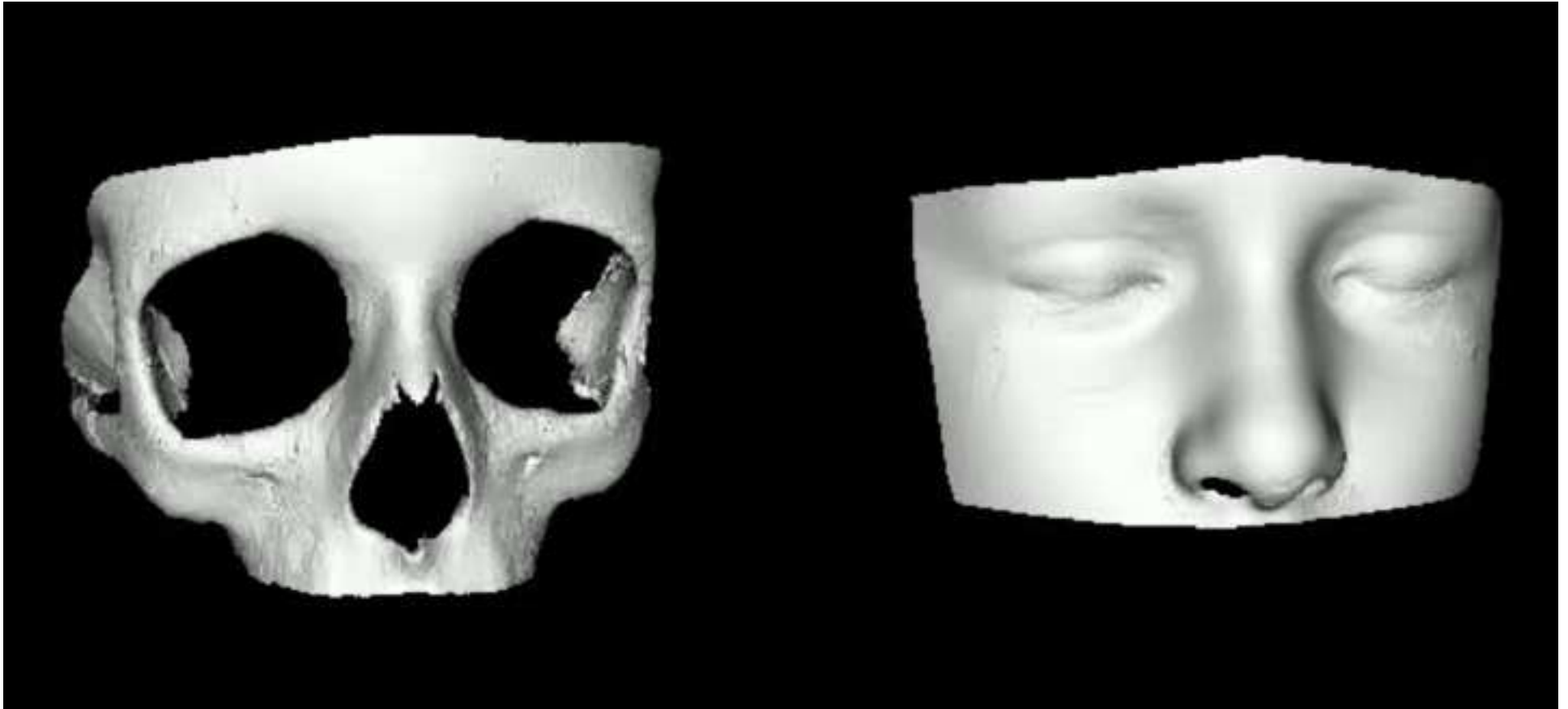
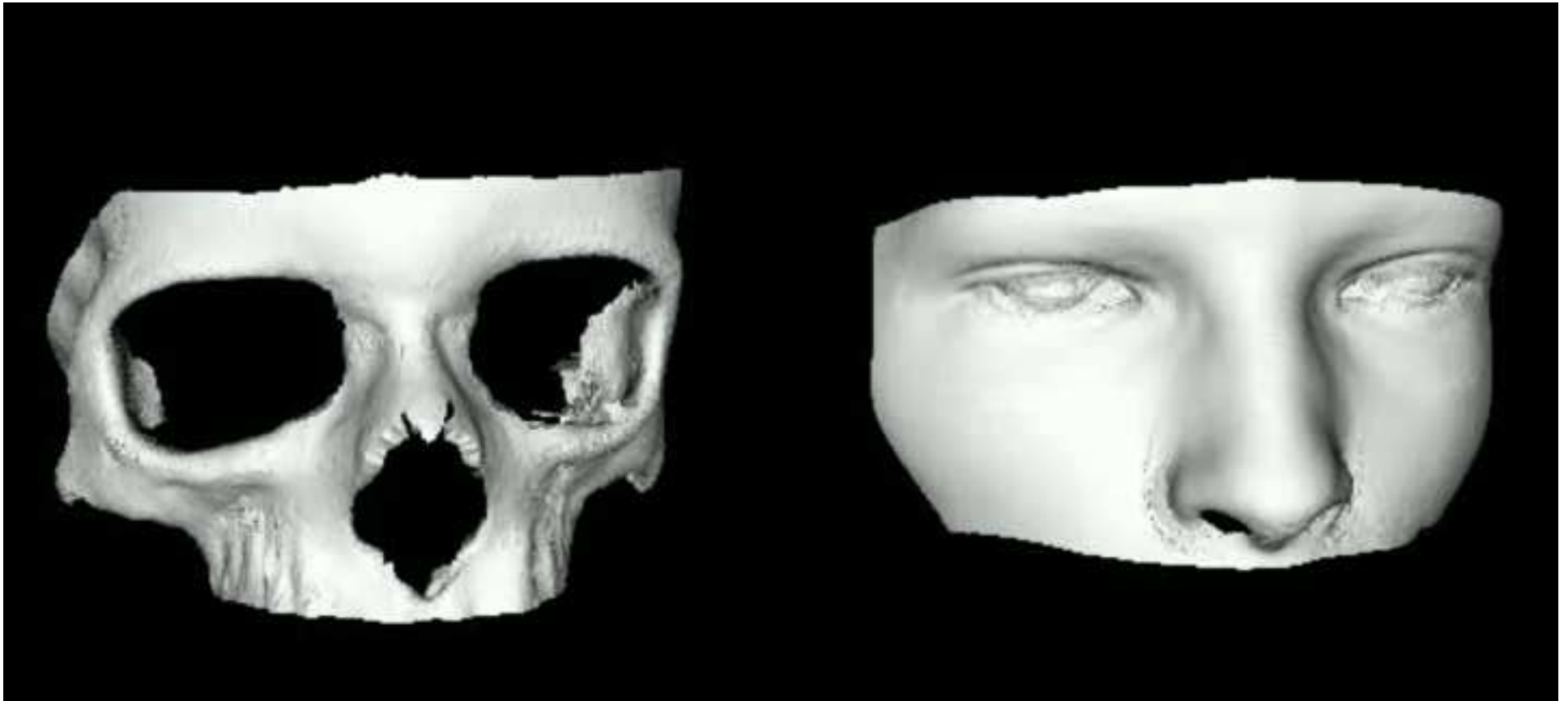


Figure 3









Video 1

[Click here to download e-component: Supplementarymovie1.mp4](#)

Video 2

[Click here to download e-component: Supplementarymovie2.mp4](#)

Video 3

[Click here to download e-component: Supplementarymovie3.mp4](#)

Video 4

[Click here to download e-component: Supplementarymovie4.mp4](#)

Supplementary figure S1

[Click here to download e-component: Supplementary figure S1.pdf](#)

Supplementary figure S2

[Click here to download e-component: Supplementary figure S2.pdf](#)

Supplementary figure S3

[Click here to download e-component: Supplementary figure S3.pdf](#)